JACS Au
AN OPEN ACCESS JOURNAL OF THE AMERICAN CHEMICAL SOCIETY



pubs.acs.org/jacsau
Article

# Synthetic $\alpha$-Helical Nanopore Reactor for Chemical Sensing

Anjali Devi Das, Vidhu K, Smitha Devi S, and Kozhinjampara R Mahendran*

Cite This: JACS Au 2023, 3, 2467−2477

Read Online

ACCESS | Metrics & More | Article Recommendations | Supporting Information

**ABSTRACT:** The use of nanopores for the single-molecule sensing of folded proteins and biomacromolecules has recently gained attention. Here, we introduce a simplified synthetic $\alpha$-helical transmembrane pore, pPorA, as a nanoreactor and sensor that exhibits functional versatility comparable to that of engineered protein and DNA nanopores. The pore, built from the assembly of synthetic 40-amino-acid-long peptides, is designed to contain cysteine residues within the lumen and at the pore terminus for site-specific chemical modification probed using single-channel electrical recordings. The reaction of the pore with differently charged activated thiol reagents was studied, wherein positively charged reagents electrophoretically driven into the pore resulted in pore blocking in discrete steps upon covalent bond formation. The asymmetric blockage patterns resulting from cis and trans-side addition of reagents reveal the pore orientation in the lipid membrane. Furthermore, activated PEG thiols covalently blocked the pores over a longer duration in a charge-independent manner, establishing the large diameter and orientation of the formed pores. While the covalent binding of thiol reagents caused a drop in the pore conductance, cationic cyclic octasaccharides produced time-resolved translocation events, confirming the structural flexibility and tunability of the pores. The ability of the pore to accommodate large analytes and the considerable current amplitude variation following bond formation events are promising for developing platforms to resolve multistep chemical reactions at the single-molecule level for applications in synthetic nanobiotechnology.

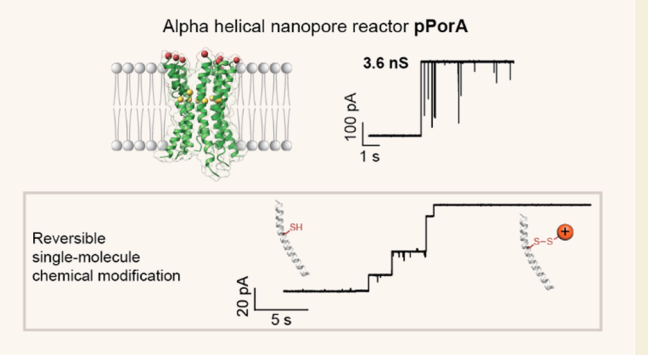


**KEYWORDS:** *nanopore, thiol reagents, current blockage, α-helical, single-channel, chemical modification*

## INTRODUCTION

Nanopore sensing has emerged as a powerful tool for single-molecule detection.[1,2] Following the initial work on the stochastic sensing of ions and small molecules and the successes of nanopore-based DNA sequencing, nanopore technology has found broader applications in molecular sensing.[3−5] More recently, nanopore technology has demonstrated considerable potential in single-molecule proteomics.[6−14] Precision-engineered pores are crucial for these applications, and progress in this area will continue to expand the potential of nanopore technology.[1,15−17] Another significant challenge in nanopore design has been achieving pores of high selectivity for ions and small molecules as seen with natural ion channels.[1] There is currently a need for the development of uniform and large-diameter pores for the selective sensing of analytes in biosensing applications. Thus, far, much of the focus has been made on engineering beta-barrel and DNA-origami pores.[18−21] Pores with an $\alpha$-helical transmembrane section, however, show high flexibility in their oligomer assembly and are more amenable to modulation in size, geometry, and selectivity than beta-barrel pores, presenting a promising platform for engineering nanopore sensors.[22−24] Nevertheless, the engineering of $\alpha$-helical transmembrane pores has remained relatively underexplored due to the significant challenges in balancing the hydrophobic and hydrophilic interactions to prevent complex nonspecific associations in the lipid membrane. Recently, advanced computational designs[25,26] and the modulation of natural assemblies have been exploited to build functional transmembrane structures.[27] We recently presented the first report of a large functional and ion-selective $\alpha$-helical nanopore made from the self-assembly of synthetic peptides based on the natural PorACj assembly.[28,29] In addition to their facile synthesis and autonomous assembly, these pores could be exploited for the charge-selective sensing of charged cyclic sugars and polypeptides.[30]

The nanopore approach has also extended beyond stochastic sensing and sequencing applications.[3,31] For example, covalent chemical reactions occurring on the interior walls of biological nanopores have been characterized at the single-molecule level with high temporal resolution.[32,33] This "nanoreactor"

Received: May 3, 2023
Revised: July 15, 2023
Accepted: July 18, 2023
Published: August 23, 2023

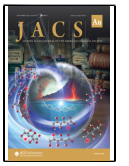

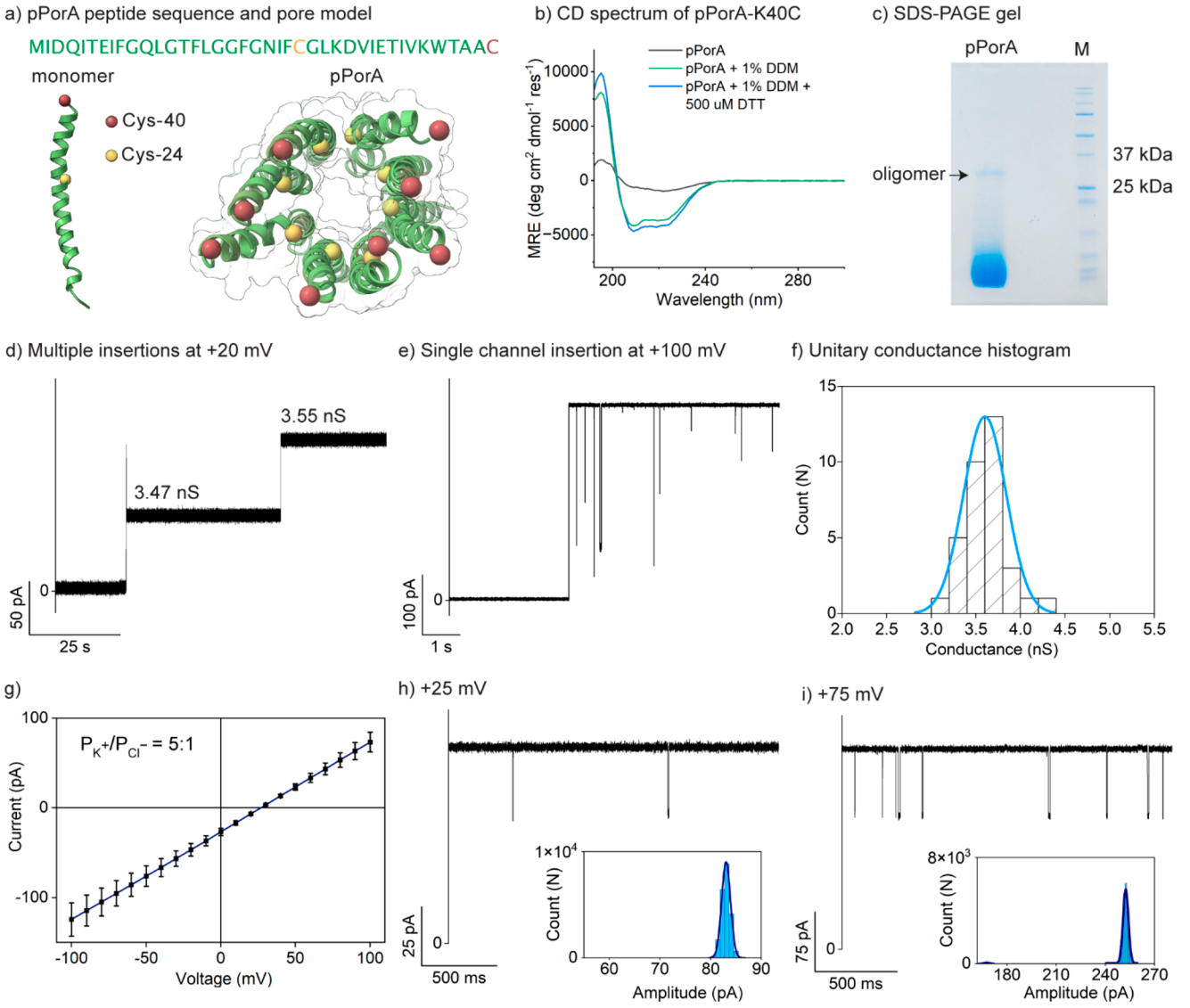


**Figure 1.** Structure and biophysical and electrical properties of pPorA. (a) pPorA peptide sequence and modeled structure of pPorA (top view). (b) Circular dichroism spectra of 100 $\mu$M pPorA peptides in phosphate-buffer without detergent (black line), with 1% DDM (green line), and 1% DDM and 500 $\mu$M dithiothreitol (blue line). The signals were recorded at 25 °C. (c) pPorA peptides after sodium dodecyl sulfate-polyacrylamide gel electrophoresis. The arrow indicates the band corresponding to the autonomously assembled pPorA oligomers. (d) Electrical recording of multiple insertions of pPorA into a planar bilayer at +20 mV and corresponding conductance values. (e) Single pPorA insertion at +100 mV. (f) Unitary conductance histogram at +50 mV. The mean conductance was obtained by fitting the distribution to a Gaussian ($n$ = 37). (g) Reverse potential obtained from the $I-V$ curve of a single pPorA pore in asymmetric buffer (1 M KCl cis and 0.15 M KCl trans at pH 7.4). Electrical recordings of single pPorA reconstituted in a lipid bilayer at (h) + 25 mV and (i) + 75 mV. Insets show the corresponding all points current–amplitude histograms. The current signals were recorded with a low pass filter frequency of 2 kHz and sampled at 10 kHz. All single-channel recordings were conducted in 1 M KCl electrolyte containing 10 mM HEPES at pH 7.4.

approach offers several advantages, such as the ability to examine intermediate steps occurring in a reaction including those that are not rate-limiting.[34,35] Covalent modification also provides a technique to identify the absolute orientation of nanopores reconstituted in lipid membranes, for which direct evidence from biophysical characterization is challenging.[36] The targeted modification of specific residues using blockers is also useful to identify the ion current pathway in the development of new pores for sensing applications. However, currently available nanoreactors have drawbacks such as low event amplitude accompanying bond-formation events and the significant challenges required to introduce reactive sites into biological pores.[37,38]

In the current work, we introduce a synthetic $\alpha$-helical transmembrane barrel as a nanoreactor responding to covalent bond formation at the single-molecule level with a high variation in current amplitude. The 40-amino-acid long peptide based on the porin PorACj of *Corynebacterium jeikeium* is designed to contain two cysteine residues available for site-specific covalent modification.[39] The peptides self-assemble into barrels that insert into lipid membranes to form large, functional, cation-selective pores. We investigated the interaction of the cysteine residues in the pores with activated thiol reagents using high-resolution single-channel electrical recordings to demonstrate their potential as a nanoreactor and nanopore sensor. Using targeted covalent modification of the cysteine residues by the asymmetric addition of activated thiol


https://doi.org/10.1021/jacsau.3c00221
JACS Au 2023, 3, 2467–2477

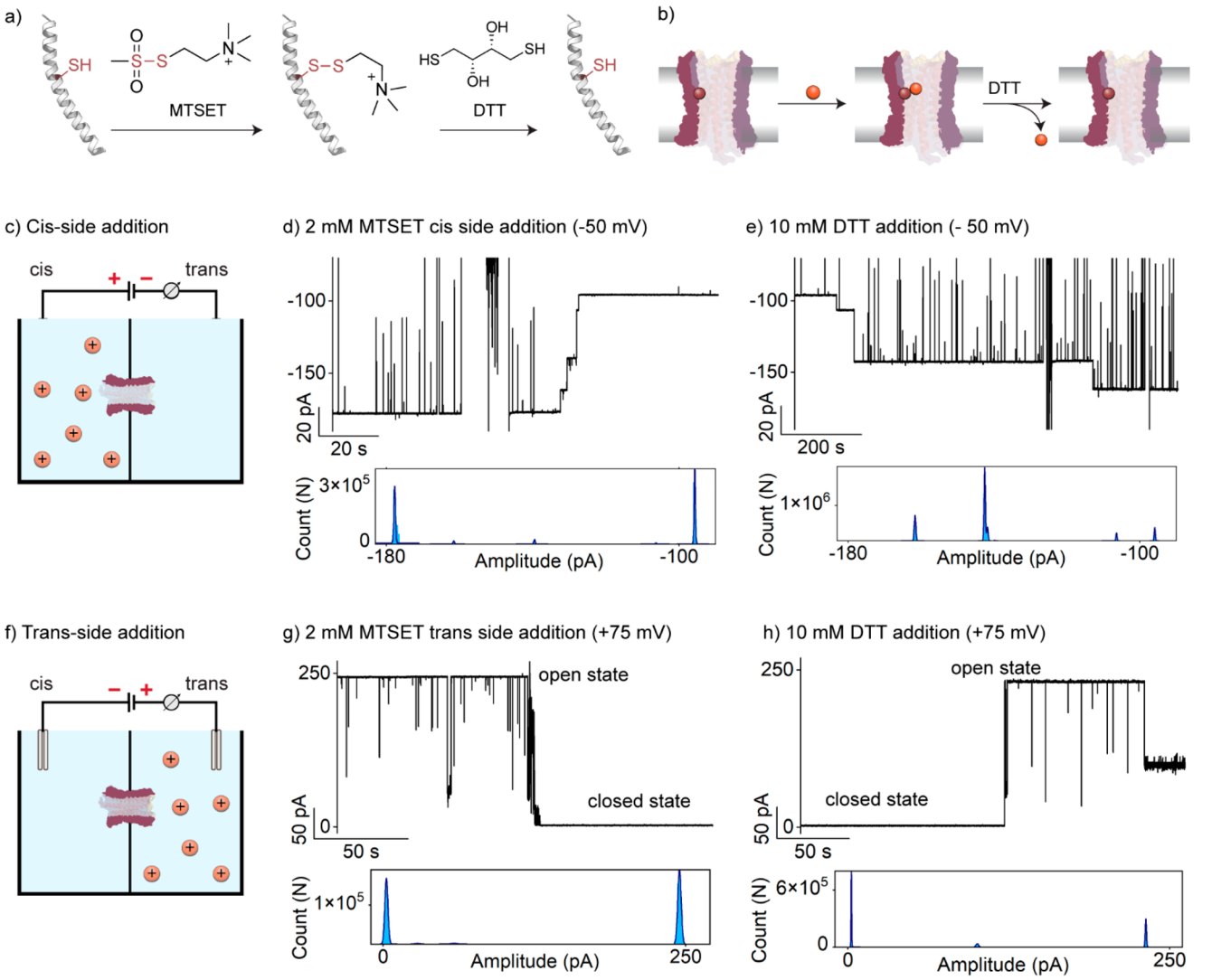


**Figure 2.** Reaction of pPorA with the positively charged MTSET. (a) Schematic of reaction of thiol side chains with MTS reagents and bond cleavage upon addition of DTT to a single peptide with 2-(trimethylammonium)ethylmethanethiosulfonate (MTSET) as representative molecule (b) Schematic of reaction leading to blockage of ion-flow and resulting current blockade. (c) Schematic of cis-side addition of MTSET. The negative voltage drives the positively charged MTSET into the pore. (d) Electrical recording of single pPorA reconstituted in a lipid bilayer at −50 mV after the addition of MTSET to the cis chamber and corresponding all-points histogram showing stepwise closure in pore current. (e) Electrical recording after the addition of 10 mM DTT at −50 mV showing the reopening of the pore and the corresponding all points histogram. (f) Schematic of trans-side MTSET addition. Positive voltage is applied to drive MTSET into the pore. (g) Electrical recording of single pPorA reconstituted in a lipid bilayer at +75 mV after the addition of MTSET to the trans chamber and corresponding all-points histogram showing complete closure in pore current. (h) Electrical recording after the addition of 10 mM DTT at +75 mV showing the reopening of the pore and corresponding all-points histogram. The current signals were digitally filtered at 200 Hz. All single-channel recordings were conducted in 1 M KCl electrolyte containing 10 mM HEPES at pH 7.4.

reagents to the bilayer device, we further attempted to elucidate the absolute pore orientation in the membrane.

## RESULTS

### Biophysical and Electrical Properties of pPorA Pores

The 40-amino-acid long-modified peptide (pPorA) was designed to contain two cysteine residues: one at the 40th position (C-terminus) and one at the 24th position and synthesized using solid-phase peptide synthesis (Figure 1a and Figure S1). When solubilized in phosphate buffer with 1% n-dodecyl $\beta$-D-maltoside (DDM), the peptide has an $\alpha$-helical secondary structure, as illustrated by the characteristic circular dichroism spectrum (Figure 1b). Addition of dithiothreitol (DTT) further aids solubilization by reducing intra- and intermolecular disulfide bonds between cysteine residues (Figure 1b). When the peptides were run in sodium-dodecyl sulfate-polyacrylamide gel electrophoresis (SDS-PAGE), a band with a molecular weight of approximately 35 kDa was observed, corresponding to a stoichiometry of eight monomers. This indicates the preoligomerization of the peptide in detergent micelles into the octameric pore-forming species, which is highly advantageous for purification (Figure 1c and Figure S2).

The corresponding gel band was subsequently cut and extracted in PBS (8.2 mM sodium phosphate, 1.8 mM potassium phosphate, 137 mM sodium chloride, and 2.7 mM potassium chloride at pH 7.4) with 0.1% DDM. The extracted peptides were then added to planar lipid bilayers to study their


https://doi.org/10.1021/jacsau.3c00221
JACS Au 2023, 3, 2467−2477

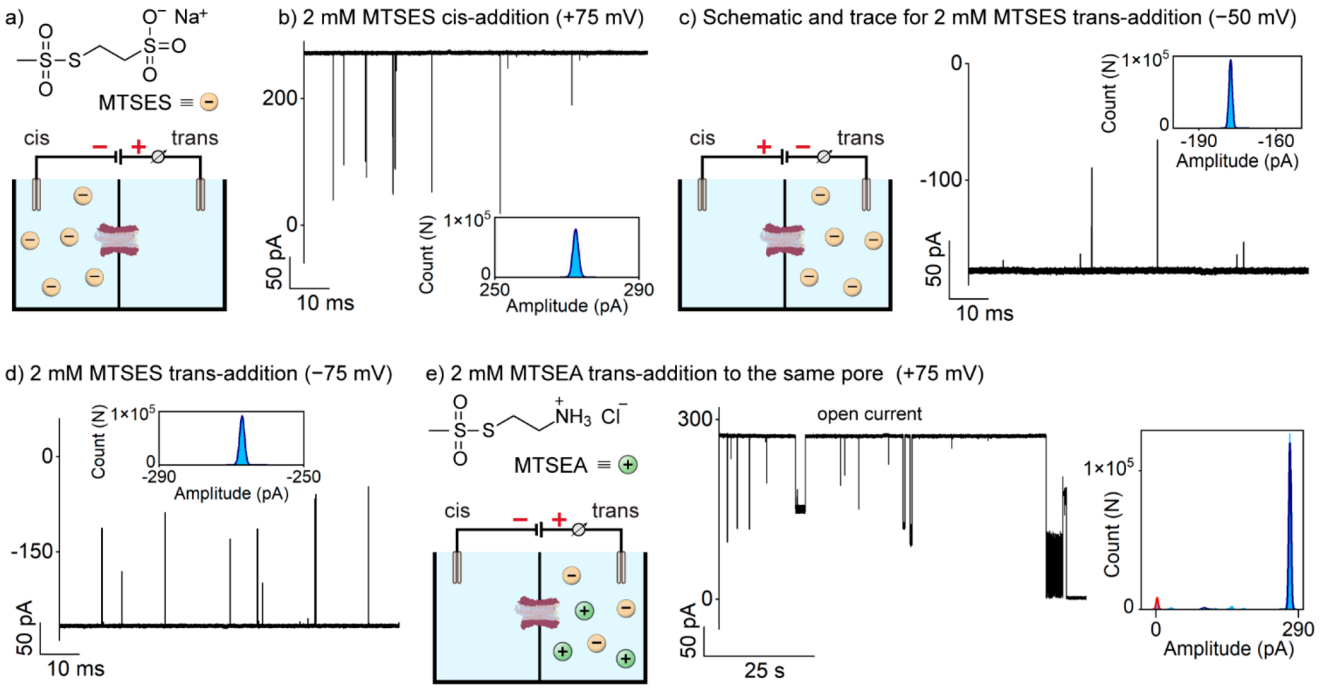


**Figure 3.** Charge-specific interaction of pPorA with negatively charged MTSES and competitive blocking experiments. (a) Structure of MTSES and schematic of cis-side MTSES addition. The positive voltage applied to the trans side drives the negatively charged MTSES into the pore. (b) Addition of 2 mM MTSES to the cis side of the pore at +75 mV does not cause pore closure. (c) Schematic and electrical trace of trans side MTSES addition with a negative applied voltage. No pore closure was observed upon the addition of 2 mM MTSES to the trans side of the pore at (c) −50 or (d) −75 mV. (e) Addition of 2 mM MTSEA to the same pore as in (d) results in pore closure. The current signals were digitally filtered at 200 Hz. All single-channel recordings were conducted in 1 M KCl electrolyte containing 10 mM HEPES at pH 7.4.

pore-forming activity using single-channel electrical recordings. The isolated oligomeric species (~35 kDa band) was found to insert into 1,2-diphytanoyl-*sn*-glycero-3-phosphocholine (DPhPC) planar lipid bilayers easily at voltages ranging from +10 to +150 mV to form stable pores (Figure 1d, e). The pPorA pore has a mean unitary conductance ($G$) of 3.60 ± 0.24 nS at +50 mV based on the statistical analysis of $n$ = 37 pores (Figure 1f–h). The conductance of the pore varied almost linearly with applied voltage with very slight asymmetry: the current amplitude was slightly higher at positive applied voltage (Figure S3). This rectification was observed in 98% of pore insertions, suggesting a preference for a particular orientation, although the absolute pore orientation was not evident. While the gating behavior was observed to vary from pore to pore, all pores showed little to no gating at voltages of +50 mV to −50 mV and marked gating states at higher conductance (> ±150 mV). The gating behavior was also uniform at positive and negative applied voltages. Ion selectivity measurements indicated that the pore was cation-selective with a permeability ratio $P_{K^+}/P_{Cl^-}$ of 5:1 (Figure 1g and Supplementary Text). In contrast to the gel-extracted pPorA that produced stable uniform pores, the direct addition of pPorA peptides to the lipid bilayer resulted in the formation of multiple pore populations of varying conductance (Figure S4). Therefore, gel-extracted pPorA was used for all chemical modification experiments.

## Chemical Modification of the Pore with Cationic Methanethiosulfonate Reagents

In our experiments, the oligomers extracted in PBS and 0.1% DDM were added to the cis side of the chamber for pore insertion. After a single pore was reconstituted into the bilayer, the chamber was repeatedly perfused to remove excess peptides. Since the pore is shown to preferentially transport cations, we attempted the site-specific covalent modification of the thiol side chains in the pore with the positively charged 2-(trimethylammonium)ethylmethanethiosulfonate (MTSET) reagent, the structure of which is shown in the reaction schematic in Figure 2a. We first investigated the interaction of MTSET with the pore upon addition to the cis chamber of the bilayer apparatus. Since MTSET is positively charged, the experiments were conducted at negative applied voltages to permit the electrophoretic driving of the analyte into the pore, as illustrated in Figure 2c. At −50 mV, the pore remained in the open conductance state until the addition of 2 mM MTSET to the cis side. Within 20 s of addition, the pore current decreased in discrete steps until a blocked state with an average residual current (IRES%) of 42.7 ± 7.5% was attained (Table S1). The pore remained blocked and could not be opened upon applying 0 mV or positive voltage. The blocked state was rapidly attained, typically 1 to 3 min after MTSET addition at −50 and −25 mV (Figure S5). The pore closure occurred with an average of 5 to 8 well-resolved ion-current blockage steps ($n$ = 5), following which the pore remained partially closed. The eight-step closure occurred with an average residual current of 36.6 ± 0.9%. The maximum of 8 current steps observed in our experiments (Figure S6) aligns with the expected octameric pore structure based on the 35 kDa band observed in SDS PAGE. This stepwise drop in channel conductance occurs due to the formation of mixed disulfide bonds between the reagent and the cysteine groups. To confirm the specificity of the chemical modification, we therefore added the reducing agent DTT to cleave the disulfide bonds. Within minutes of the addition of 10 mM DTT and the mixing of the contents of the chamber, the pore started to


https://doi.org/10.1021/jacsau.3c00221
JACS Au 2023, 3, 2467−2477

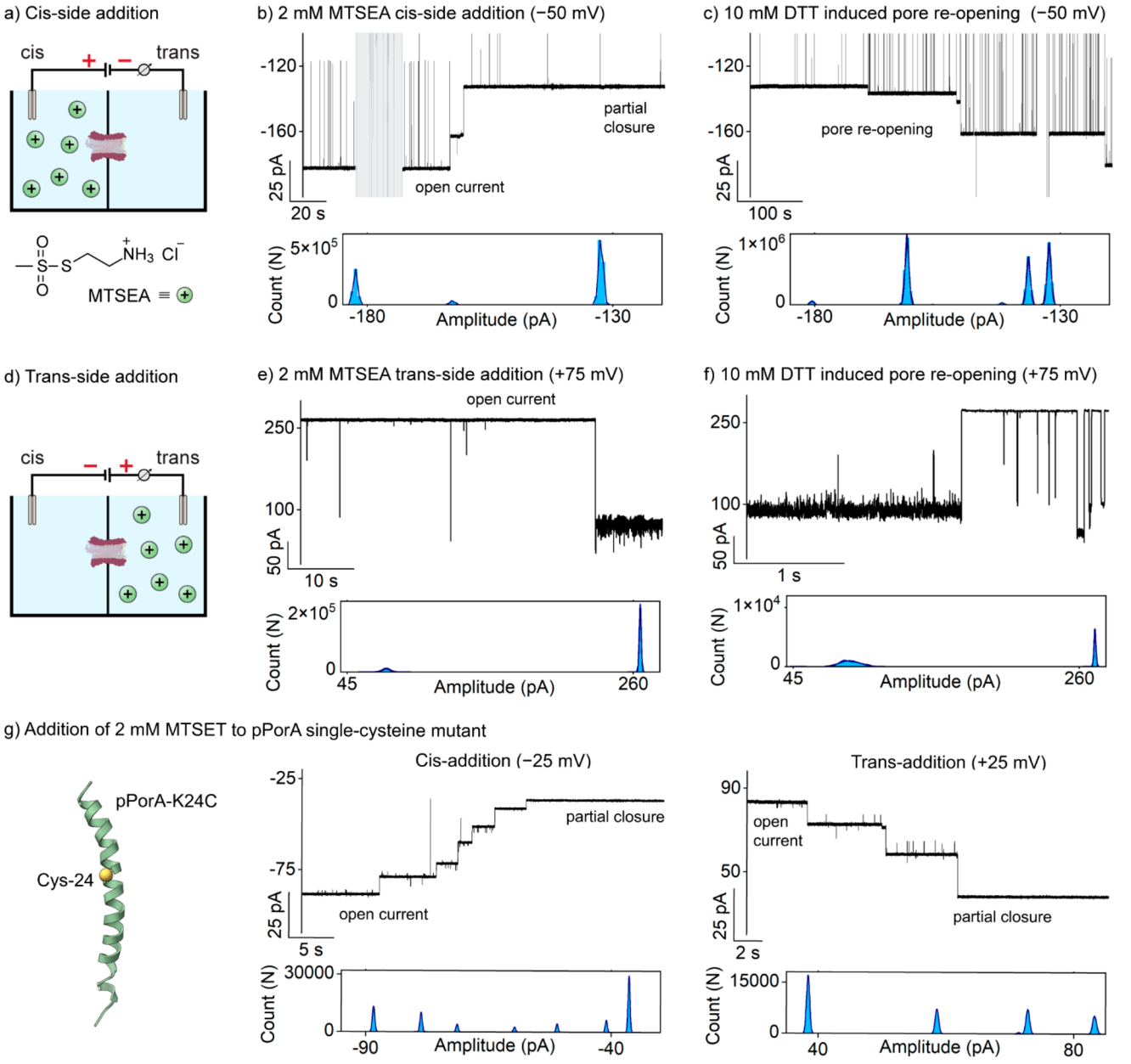


**Figure 4.** Reaction of pPorA with positively charged MTSEA and the chemical modification of pPorA-K24C. (a) Schematic of cis side MTSEA addition. The negative applied voltage drives the positively charged MTSEA into the pore. (b) Addition of 2 mM MTSEA to the cis side of the pore causing partial closure. (c) Addition of 10 mM DTT to the trans side of the pore results in reopening. (d) Schematic of trans-side MTSEA addition. The positive voltage applied to the trans side drives the positively charged MTSEA into the pore. (e) Addition of MTSEA to the trans side of the pore results in full pore closure. (f) Addition of 10 mM DTT to the trans side results in pore reopening. (g) Cis- and trans-addition of 2 mM MTSET to single cysteine mutant pPorA-K24C resulting in partial pore closure. The current signals were digitally filtered at 200 Hz. All single-channel recordings were conducted in 1 M KCl electrolyte containing 10 mM HEPES at pH 7.4.

revert to its open conductance state. This reopening process was significantly slower than the pore closure since DTT is a neutral molecule and slowly diffuses through the pore along with the ion flow.

Once the partial closure from cis-side addition was established, we investigated the pore behavior upon trans-side addition to probe the effect of adding the analyte to either side of the pore (Figure 2f). Interestingly, when 2 mM MTSET was added to the trans side, the pore closed from the open conductance state to a blocked state with a low average residual current of 2.4 ± 2.2% (Figure 2g and Table S1). The pores subsequently reopened upon the addition of 10 mM DTT (Figure 2h). We consistently observed close to complete closure upon trans-side addition, with residual current remaining <5% of the open current (Figure S7). Our results indicate that there is a clear asymmetry in the residual current resulting from the site-specific modification of the pore upon cis-side and trans-side addition of the analyte.

## Charge-Specific Interaction of pPorA and Competitive Blocking Experiments

To investigate the charge-selective interaction of the pore, we further examined the interaction with the negatively charged activated thiol reagent 2-sulfonatoethylmethanethiosulfonate (MTSES), the structure of which is shown in Figure 3a. Two


https://doi.org/10.1021/jacsau.3c00221
JACS Au 2023, 3, 2467−2477

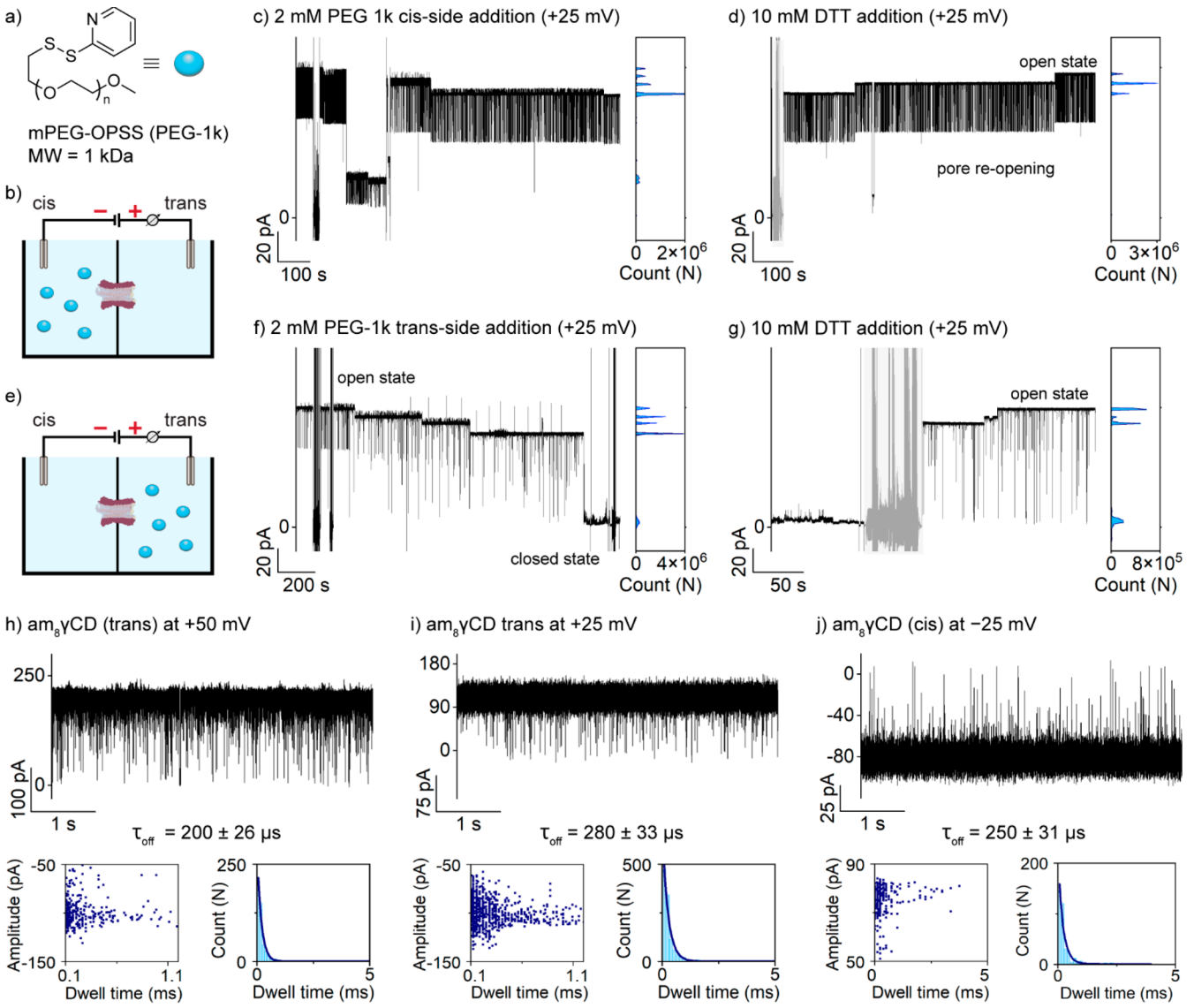


**Figure 5.** Interaction of pPorA nanoreactor with mPEG-OPSS 1k. (a) Structure of mPEG-OPSS 1k (MW = 1 kDa). (b) Schematic for cis-side addition of mPEG-OPSS at positive applied voltage. (c) Addition of 2 mM mPEG-OPSS to the cis chamber at +25 mV led to partial pore closure and corresponding all-points histogram. (d) 10 mM DTT-induced pore reopening at +25 mV and corresponding all-points histogram. (e) Schematic for trans-side addition of mPEG-OPSS at positive applied voltage. (f) Addition of 2 mM mPEG-OPSS to the trans chamber leading to full pore closure at +25 mV and corresponding all-points histogram. (g)10 mM DTT-induced pore reopening at +25 mV and corresponding histogram. Electrical recordings of single pPorA in the presence of $am_8\gamma CD$ (10 $\mu$M, trans) at (h) + 50 mV, (i) + 25 mV and j) (5 $\mu$M, cis) at −25 mV. Insets show the dwell time histograms and the scatter plots of current block amplitudes versus dwell time of CD translocation events. The current signals c and d and f and g were digitally filtered at 200 Hz. Current signals h−j were recorded with a low pass filter frequency of 10 kHz and a sampling frequency of 50 kHz. All single-channel recordings were conducted in 1 M KCl electrolyte containing 10 mM HEPES at pH 7.4.

mM MTSES was added to the cis side, and positive voltage was applied to electrophoretically drive the analyte into the pore as shown in the schematic in Figure 3a. Initially, a low voltage of +25 mV was applied, upon which no current variation was observed (Figure S8). The pore further remained in the open state when the voltage was increased to +50 mV and then to +75 mV (Figure 3b and Figure S8a). No current variation was observed for extended periods even at +75 mV (Figure S8) in all our experiments. Subsequently, 2 mM MTSES was added to the trans side of the pore with a negative applied voltage (Figure 3c). Again, no current variation was observed even upon increasing the voltage from −25 to −50 and −75 mV for extended periods (Figure 3c and Figure S8). To confirm that the thiol groups were still available for modification, we then performed competitive blocking experiments on the same pore. First, 2 mM MTSES was added to the trans side of the pore, wherein no closure was observed at negative applied voltages of up to −75 mV (Figure 3d). We then added the positively charged reagent 2-aminoethylmethanethiosulfonate hydrobromide (MTSEA) to the trans side of the same pore (Figure 3e). We then applied a voltage of +75 mV to electrophoretically drive the reagent into the pore. MTSEA addition resulted in complete pore closure with a residual current of 1.26%, consistent with the previous results of trans-side addition of MTSET and confirming the charge-selective blocking of pPorA. This result further highlights the cation-selective nature of the pore.



https://doi.org/10.1021/jacsau.3c00221
JACS Au 2023, 3, 2467−2477

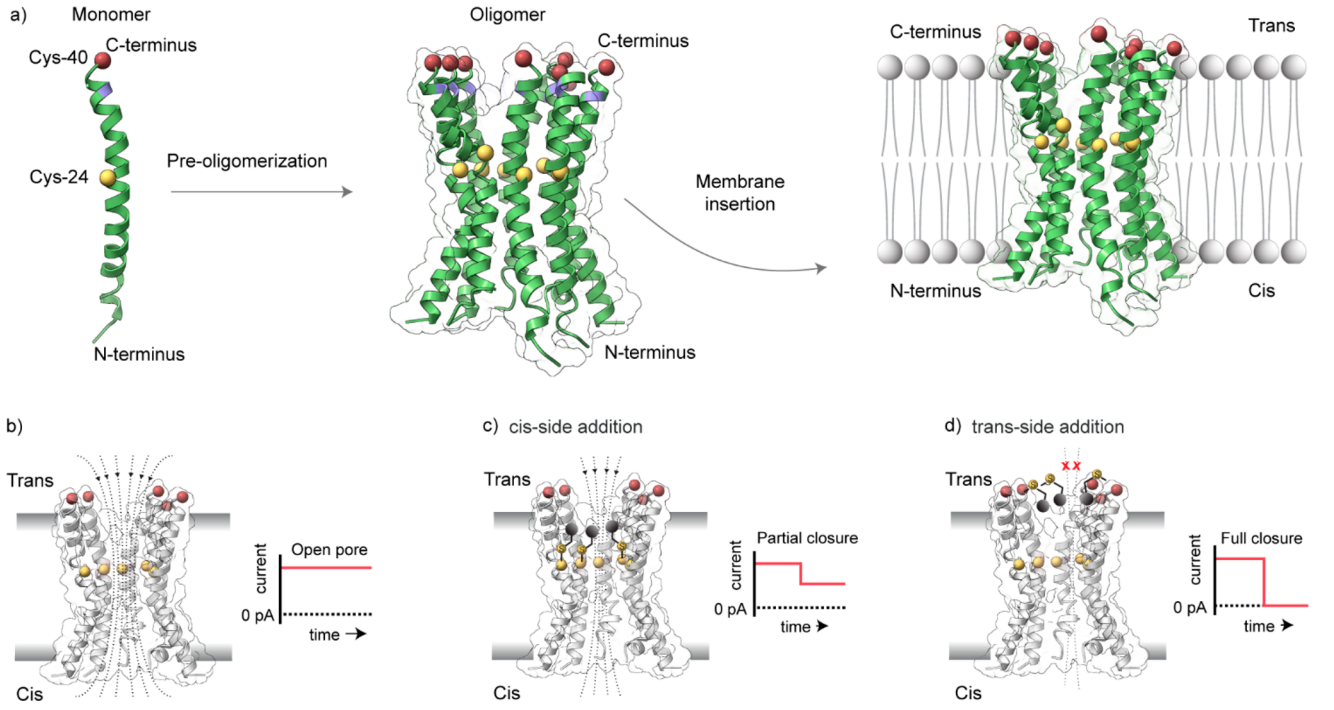


**Figure 6.** (a) Model pPorA pore formation. The pPorA monomer assembles to form a stable octameric $\alpha$-helical barrel proposed to insert into lipid bilayers in a C-terminal-first pore insertion. Model for asymmetric current blockage upon addition of thiol reagents to cis and trans side. (b) Open pore in the lipid bilayer. (c) Cis-side addition targets the cysteine residues within the pore lumen, leading to a partial drop in the open pore current. (d) Trans-side addition results in almost full pore closure.

Since MTSEA was observed to cause complete pore closure upon trans-side addition, we performed additional experiments to confirm the asymmetry in the current blockage upon chemical modification. When 2 mM MTSEA was added to the cis side of the pore at −50 mV (Figure 4a,b), stepwise pore closure occurred rapidly, starting within 40 s of MTSEA addition. A blocked state with an average residual current of 75.1 ± 2.0% was attained in less than 1 min (Figure 4b and S9). The addition of 10 mM DTT resulted in cleavage of the disulfide bonds and the pore reverted to the original open state (Figure 4c). Upon repeating the trans-side addition of 2 mM MTSEA to a pore at +75 mV (Figure 4d), a blocked state with 14.1 ± 3.7% average residual current was attained (Figure 4e). The pore reopened to its original state upon the addition of 10 mM DTT (Figure 4f). This asymmetric blockage upon cis- and trans-side addition of MTSEA is similar to or previous observation with the positively charged MTSET blocker.

We further investigated the covalent modification of the mutant pPorA-K24C, which contains a single-cysteine at the 24th position, where 2 mM MTSET was added to the cis- and trans-side of pPorA-K24C (Figure 4g and Figure S10). In the single-cysteine mutant, we observed symmetric pore closure to a partially blocked state, whereas in the double cysteine mutant asymmetric pore closure was observed. Based on these results, we suggest that the in both the single and double cysteine mutants, partial closure is caused due to chemical modification at cysteine 24th position, and that the asymmetry is related to the orientation of the pore in the lipid bilayer.

## Interaction of pPorA with Neutral Activated Thiol PEG Polymers and Cationic Cyclic Octasaccharides

We further wanted to investigate the interaction of the pores with larger polymeric reagents to probe the large diameter of the pores.[40] Therefore, we examined the interaction of the engineered cysteine residues in pPorA with the large uncharged sulfhydryl-directed polyethylene glycol polymer monomethoxy poly(ethylene glycol)-orthopyridyl disulfide-1k (mPEG-OPSS-1k, MW = 1 kDa) reagent, whose structure is shown in Figure 5a. All experiments were conducted at +25 mV since the PEG blocker diffuses into the pore along with the flow of ions with no electrophoretic pulling required (Figure 5b and e). Upon adding 2 mM mPEG-OPSS-1k to the cis compartment, we observed stepwise pore closure within 10 to 15 min (Figure 5c). The lack of electrophoretic force on the reagent manifests in the higher time scale required for the pore closure compared to that of the positively charged MTS reagents. The current decreased from the open conductance state at +25 mV to a blocked state with a residual current of 82.55%. Subsequently, after adding 10 mM DTT to the trans side the pore reopened in 5−10 min (Figure 5d). We further observed that the addition of 2 mM mPEG-OPSS to the trans chamber resulted in almost complete pore closure with a residual current of 4.30% at +25 mV (Figure 5f). The pore remained closed for over 10 min and started to reopen immediately after adding 10 mM DTT, attaining the original open state within 3 min (Figure 5g and Figure S11).

The blockage pattern observed upon the asymmetric addition was similar to that observed upon the addition of the positively charged MTSET and MTSEA reagents (Tables S1). However, the residual current resulting from the cis-side addition of mPEG-OPSS is observed to be higher than that upon the addition of MTS reagents (Table S2), consistent with the large size of the polymer hindering its entrance into the pore lumen.

Finally, we examined the interaction of positively charged cyclodextrins with pPorA. The addition of 10 $\mu$M cationic octasaccharide $am_8\gamma CD$, to the trans side of the pore, resulted in time-resolved ion-current blockages at positive applied


https://doi.org/10.1021/jacsau.3c00221
JACS Au 2023, 3, 2467−2477

voltages of +50 mV and +25 mV as shown in Figure 5h and i, respectively. No blockage events were observed when the voltage was reversed, demonstrating that the applied voltage acts as a force that draws the charged CDs toward the negatively charged residues in the pore to facilitate their interaction (Figure S12c). The CDs interact with the trans-side of the pore to give well-defined blockage events with a dwell time of ∼280 $\mu$s at +25 mV and ∼200 $\mu$s at +50 mV. Next, the addition of 5 $\mu$M cationic $am_8\gamma$CD to the cis side of the pore resulted in time-resolved ion current blockages at negative voltages (Figure 5j): $am_8\gamma$CD shows blockage events with a dwell time of ∼250 $\mu$s at +25 mV and ∼190 $\mu$s at +50 mV (Figure 5j and Figure S12). The slight decrease in the dwell time of $am_8\gamma$CD binding with increasing voltage indicates that the CDs translocate through the pores, in agreement with the cation-selective nature of the pore. The $am_8\gamma$CD noncovalently binds and subsequently translocates through the pore upon the application of electrostatic force. The blockage pattern resulting from this transient interaction is distinct from that observed upon site-specific covalent modification of the pores, in which a permanent drop in conductance is observed, which can only be reversed by adding a reducing agent.

## DISCUSSION

Here, we rationally designed and engineered a synthetic pore, pPorA, based on the model structure of the natural PorACj porin for single-molecule chemical sensing. The spontaneous assembly of the monomeric pPorA peptides in detergent micelles to form preoligomers permits the extraction of the oligomer from the SDS-PAGE gel: a straightforward process that is highly advantageous for the single-step purification of pPorA. Adding DTT releases further monomers that assemble in the presence of DDM micelles to form the pore-oligomeric species that form stable pores in the planar lipid bilayers. In pPorA, the current asymmetry at positive voltages, although minor, indicates that one of two preferred orientations of pPorA is preferred 98% of the time ($n$ = 50). However, the direction of the preferred orientation, which is crucial for applications in nanopore sensing, remains unclear. The orientation of a protein when it inserts into a lipid membrane can depend on various factors, such as the amino acid sequence. In the planar lipid bilayers used in single-channel experiments, the N-terminus or C-terminus may insert first if it contains hydrophobic amino acids or a transmembrane domain that anchors the protein into the membrane. In biological pores, the two orientations can typically be distinguished by the current−voltage asymmetry or the higher voltage-dependent gating observed at the positive or negative applied potential.[36,41] The pPorA peptide used in this study contains two cysteine residues available for site-specific covalent modification: one within the pore lumen and one at the terminal pore entrance. Depending on the preferred orientation of the pore in the lipid bilayers, the terminal cysteine residues remain exposed in the trans or cis chamber (Figure 6a). Based on the distinct blockage pattern caused by the asymmetric addition of thiol reagents to the pore, we propose an assembly mechanism and a model for the insertion and orientation of these pores in the lipid membrane (Figure 6b−d). The partial closure observed upon cis-side addition to both the single- and double- cysteine mutants suggests that the reactive sites participating upon cis-side addition must be the cysteines located within the pore lumen. In contrast, the full-closure of the double-cysteine mutant upon trans-side addition, which is not observed in the single-cysteine mutant, is therefore attributed to the reaction of the terminal cysteine residues absent in the single-cysteine mutant. Our findings therefore suggest that the terminal cysteines are exposed in the trans chamber of the bilayer apparatus as shown in the schematic in Figure 6d. This is further supported by the higher residual current resulting from the addition of the larger PEG polymers to the pPorA. Based on the convention followed in our experiments, pPorA is added to the cis side of the bilayer apparatus. Therefore, pore insertion should occur following a C-terminus-first route. This hypothesis is supported by the presence of an aromatic tryptophan residue at the 36th position, which has been shown to participate in membrane anchorage.[42,43] C-terminus-first pore insertion also results in a pore orientation where the cis-facing side of the pore contains more acidic residues than the trans-facing side of the pore.

Transmembrane pores based on $\alpha$-helices are a highly sort after motif in nanobiotechnology and synthetic chemical biology.[44−46] While there have been reports of soluble $\alpha$-helical barrels made from designed synthetic peptides, there are significantly fewer reports of synthetic membrane proteins, including those built from de novo design and by adapting existing natural structures.[45,47] Incorporating multiple cysteine mutations in biological proteins can lead to the formation of aggregates which hinders isolation and purification.[28] pPorA, an autonomous-helix-based transmembrane assembly presents a new class of synthetic nanoreactors that show several advantages compared to biological and DNA pores, including ease of synthesis, facile purification, unusually large conductance, and specificity for molecules. Furthermore, reproducing the ion selectivity of natural biological ion channels in artificial nanopore systems has long since been a significant challenge, and achieving this goal offers high technological potential.[48] pPorA shows selectivity to positively charged MTS reagents over negatively charged reagents, providing a platform for engineering pPorA pores to conduct specific ions selectively. The large size of the pore is especially relevant for examining single-molecule covalent chemistry, in which the ability to accommodate large analytes is highly desirable. The ability to elucidate the absolute orientation upon reconstitution in lipid bilayers, which has thus far been a challenge, further opens avenues for the application of the versatile peptide pores in synthetic biology, including the design of dimeric pores and the inclusion of photoreactive elements that may be useful for light-triggered transport.[49,50]

## CONCLUSION

In this study, we introduce a chemically synthesized $\alpha$-helical pore, pPorA, as a nanoreactor. We studied the interaction of the thiol side chains of pPorA by targeted covalent modification with sulfhydryl-directed reagents and were able to resolve individual bond-formation events within the pore. We further showed the charge-selective nature of the pore and differentiated covalent modification events from electrophoretically driven translocation. By targeting dual residues in the pore lumen, the effect of covalent modification of the terminal cysteines and interior cysteines was clearly differentiated. Analysis of the asymmetry of chemical modification further revealed that the peptides are arranged in parallel with their N-termini on the cis side of the membrane, providing insight into the membrane assembly mechanism of the pore. The pPorA nanoreactors are versatile motifs in which reactive sites can be incorporated during synthesis, thus potentially


https://doi.org/10.1021/jacsau.3c00221
JACS Au 2023, 3, 2467−2477

expanding the range of single-molecule chemistry that can be examined using the nanopore approach.

## METHODS

### Single-Channel Electrical Recordings

Planar lipid bilayer recordings were carried out by using bilayers of 1,2-diphytanoyl-*sn*-glycero-3-phosphocholine (DPhPC, Avanti Polar Lipids) formed across an aperture (~70 $\mu$m in diameter) in a 25 $\mu$m thick polytetrafluoroethylene (Teflon) film (Goodfellow, Cambridge), separating the apparatus into two compartments defined as cis and trans, each with a capacity of 600 $\mu$L). Each side of the aperture was pretreated with a solution of hexadecane in *n*-pentane (1 $\mu$L, 5 mg mL$^{-1}$) on each side, following which both compartments were filled with electrolyte (1 M KCl, 10 mM HEPES, pH 7.4). A solution of DPhPC in *n*-pentane (2 $\mu$L, 5 mg mL$^{-1}$) was added to both sides, following which the solvent was allowed to evaporate. Planar lipid bilayers were formed by lowering and raising the electrolyte level to bring the two lipid surface monolayers together at the aperture. The pPorA pores were formed by adding a solution of the peptide gel extract in 0.1% DDM (1 $\mu$L, 100 $\mu$g mL$^{-1}$) to the cis side of the chamber under an applied potential. Prior to addition, the solution was briefly incubated with 1 mM DTT. The cis compartment was connected to the grounded electrode, and the trans compartment was attached to the working electrode. A potential difference was applied through a pair of Ag/AgCl electrodes set in 3% agarose containing 3 M KCl. The ion selectivity of pores was measured by using a KCl salt gradient applied across the bilayer chambers (1 M cis/0.15 M trans). Solutions of MTSET, MTSES, MTSEA, and PEG-OPSS-1k were prepared immediately prior to use. The current was amplified by using an Axopatch 200B amplifier, digitized with a Digidata 1550B, and recorded with pClamp 11.0 acquisition software (Molecular Devices, CA). MTS and PEG-OPSS data were recorded with a low pass filter frequency of 2 kHz and a sampling frequency of 10 kHz. Interaction of pPorA with am$_8\gamma$CD was recorded with a low pass filter frequency of 10 kHz and a sampling frequency of 50 kHz. The data were analyzed with pClamp (ver. 11.2, Molecular Devices, CA) and plotted using OriginPro 2023 (OriginLab).

## ASSOCIATED CONTENT

### Supporting Information

The Supporting Information is available free of charge at https://pubs.acs.org/doi/10.1021/jacsau.3c00221.

Materials and methods, peptide characterization data (mass spectra, SDS-PAGE), IV curves, residual current tables, electrical recordings of chemical modification experiments (PDF)

## AUTHOR INFORMATION


### Corresponding Author

**Kozhinjampara R Mahendran** − *Membrane Biology Laboratory, Rajiv Gandhi Centre for Biotechnology, Thiruvananthapuram, India 695014;* orcid.org/0000-0003-2549-9250; Email: mahendran@rgcb.res.in

### Authors

**Anjali Devi Das** − *Membrane Biology Laboratory, Rajiv Gandhi Centre for Biotechnology, Thiruvananthapuram, India 695014*

**Vidhu K** − *Membrane Biology Laboratory, Rajiv Gandhi Centre for Biotechnology, Thiruvananthapuram, India 695014*

**Smitha Devi S** − *Membrane Biology Laboratory, Rajiv Gandhi Centre for Biotechnology, Thiruvananthapuram, India 695014*

Complete contact information is available at: https://pubs.acs.org/10.1021/jacsau.3c00221


### Author Contributions

A.D. and K.R.M. conceived the idea and designed the project. A.D. performed all single-channel recordings and biophysical characterization. A.D. and K.R.M. conducted data analysis. V.D. supported data analysis and MTS experiments. A.D. and K.R.M. wrote the manuscript. K.R.M. supervised the study. All authors have approved the final version of the manuscript. CRediT: **Anjali Devi Das** conceptualization, data curation, formal analysis, methodology, validation, writing-original draft, writing-review & editing; **Vidhu K** formal analysis, validation; **Smitha Devi S** formal analysis, validation; **Kozhinjampara R Mahendran** conceptualization, data curation, formal analysis, investigation, project administration, resources, supervision, writing-original draft, writing-review & editing.

### Notes

The authors declare no competing financial interest.

## ACKNOWLEDGMENTS

This work was supported by research grants from the Department of Biotechnology, India (BT/PR34466/BRB/10/1830/2019 and BT/PR41427/BRB/10/1959/2020). KRM acknowledges the research grant of the Science & Engineering Research Board (SERB) and the Department of Science and Technology (DST), India (CRG/2021/000622). We thank Professor Chandrabhas Narayana (Director, RGCB) for supporting the project.

## ABBREVIATIONS

$\alpha$-HL, $\alpha$-hemolysin; am$_8\gamma$CD, octakis-(6-amino-6-deoxy)-$\gamma$-cyclodextrin octahydrochloride; DDM, n-dodecyl $\beta$-D-maltoside; DTT, dithiothrietol; MTS, methanethiosulfonate; MTSEA, 2-aminoethylmethanethiosulfonate hydrobromide; MTSES, 2-sulfonatoethylmethanethiosulfonate sodium salt; (am8$\gamma$CD MTSET, 2-(trimethylammonium)-ethylmethanethiosulfonate; mPEG-OPSS, monomethoxypoly-(ethylene glycol)-orthopyridyl disulfide; SDS-PAGE, sodium-dodecyl sulfate-polyacrylamide gel electrophoresis

## REFERENCES


(1) Ayub, M.; Bayley, H. Engineered Transmembrane Pores. *Curr. Opin Chem. Biol.* **2016**, *34*, 117−126.

(2) Keyser, U. F. Controlling Molecular Transport through Nanopores. *Journal of the Royal Society Interface* **2011**, *8*, 1369−1378.

(3) Ying, Y. L.; Hu, Z. L.; Zhang, S.; Qing, Y.; Fragasso, A.; Maglia, G.; Meller, A.; Bayley, H.; Dekker, C.; Long, Y. T. Nanopore-Based Technologies beyond DNA Sequencing. *Nature Nanotechnology* **2022**, *17*, 1136−1146.

(4) Kasianowicz, J. J.; Balijepalli, A. K.; Ettedgui, J.; Forstater, J. H.; Wang, H.; Zhang, H.; Robertson, J. W. F. Analytical Applications for Pore-Forming Proteins. *Biochim Biophys Acta Biomembr* **2016**, *1858* (3), 593−606.

(5) Takeuchi, N.; Hiratani, M.; Kawano, R. Pattern Recognition of MicroRNA Expression in Body Fluids Using Nanopore Decoding at Subfemtomolar Concentrations. *JACS Au* **2022**, *2* (8), 1829−1838.

(6) Hu, Z.; Huo, M.; Ying, Y.; Long, Y. Biological Nanopore Approach for Single-Molecule Protein Sequencing. *Angew. Chem., Int. Ed.* **2021**, *60* (27), 14738−14749.

(7) Thakur, A. K.; Movileanu, L. Real-Time Measurement of Protein-Protein Interactions at Single-Molecule Resolution Using a Biological Nanopore. *Nat. Biotechnol.* **2019**, *37* (1), 96−101.

(8) Ouldali, H.; Sarthak, K.; Ensslen, T.; Piguet, F.; Manivet, P.; Pelta, J.; Behrends, J. C.; Aksimentiev, A.; Oukhaled, A. Electrical Recognition of the Twenty Proteinogenic Amino Acids Using an Aerolysin Nanopore. *Nat. Biotechnol.* **2020**, *38* (2), 176−181.
(9) Derrington, I. M.; Craig, J. M.; Stava, E.; Laszlo, A. H.; Ross, B. C.; Brinkerhoff, H.; Nova, I. C.; Doering, K.; Tickman, B. I.; Ronaghi, M.; Mandell, J. G.; Gunderson, K. L.; Gundlach, J. H. Subangstrom Single-Molecule Measurements of Motor Proteins Using a Nanopore. *Nat. Biotechnol.* **2015**, *33* (10), 1073−1075.
(10) Piguet, F.; Ouldali, H.; Pastoriza-Gallego, M.; Manivet, P.; Pelta, J.; Oukhaled, A. Identification of Single Amino Acid Differences in Uniformly Charged Homopolymeric Peptides with Aerolysin Nanopore. *Nat. Commun.* **2018**, *9* (1), 966.
(11) Thakur, A. K.; Movileanu, L. Real-Time Measurement of Protein−Protein Interactions at Single-Molecule Resolution Using a Biological Nanopore. *Nature Biotechnology 2018 37:1* **2019**, *37* (1), 96−101.
(12) Yan, S.; Zhang, J.; Wang, Y.; Guo, W.; Zhang, S.; Liu, Y.; Cao, J.; Wang, Y.; Wang, L.; Ma, F.; Zhang, P.; Chen, H. Y.; Huang, S. Single Molecule Ratcheting Motion of Peptides in a Mycobacterium Smegmatis Porin A (MspA) Nanopore. *Nano Lett.* **2021**, *21* (15), 6703−6710.
(13) Brinkerhoff, H.; Kang, A. S. W.; Liu, J.; Aksimentiev, A.; Dekker, C. Multiple Rereads of Single Proteins at Single-Amino Acid Resolution Using Nanopores. *Science (1979)* **2021**, *374* (6574), 1509−1513.
(14) Lucas, F. L. R.; Versloot, R. C. A.; Yakovlieva, L.; Walvoort, M. T. C.; Maglia, G. Protein Identification by Nanopore Peptide Profiling. *Nat. Commun.* **2021**, *12* (1), 1−9.
(15) Howorka, S. Building Membrane Nanopores. *Nature Nanotechnology* **2017**, *12*, 619−630.
(16) Zhu, J.; Avakyan, N.; Kakkis, A.; Hoffnagle, A. M.; Han, K.; Li, Y.; Zhang, Z.; Choi, T. S.; Na, Y.; Yu, C. J.; Tezcan, F. A. Protein Assembly by Design. *Chem. Rev.* **2021**, *121* (22), 13701−13796.
(17) Li, M.-Y.; Ying, Y.-L.; Yu, J.; Liu, S.-C.; Wang, Y.-Q.; Li, S.; Long, Y.-T. Revisiting the Origin of Nanopore Current Blockage for Volume Difference Sensing at the Atomic Level. *JACS Au* **2021**, *1* (7), 967−976.
(18) Liu, L.; Wu, H. C. DNA-Based Nanopore Sensing. *Angewandte Chemie - International ed.* **2016**, *55*, 15216−15222.
(19) Hu, Z. L.; Huo, M. Z.; Ying, Y. L.; Long, Y. T. Biological Nanopore Approach for Single-Molecule Protein Sequencing. *Angew. Chem., Int. Ed.* **2021**, *60* (27), 14738−14749.
(20) Crnković, A.; Srnko, M.; Anderluh, G. Biological Nanopores: Engineering on Demand. *Life* **2021**, *11* (1), 27.
(21) Diederichs, T.; Pugh, G.; Dorey, A.; Xing, Y.; Burns, J. R.; Hung Nguyen, Q.; Tornow, M.; Tampé, R.; Howorka, S. Synthetic Protein-Conductive Membrane Nanopores Built with DNA. *Nat. Commun.* **2019**, *10* (1), 5018.
(22) Crnkovi′c, A. C.; Srnko, M.; Anderluh, G. Biological Nanopores: Engineering on Demand. *Life* **2021**, *11* (1), 27.
(23) Eifler, N.; Vetsch, M.; Gregorini, M.; Ringler, P.; Chami, M.; Philippsen, A.; Fritz, A.; Müller, S. A.; Glockshuber, R.; Engel, A.; Grauschopf, U. Cytotoxin ClyA from Escherichia Coli Assembles to a 13-Meric Pore Independent of Its Redox-State. *EMBO J.* **2006**, *25* (11), 2652−2661.
(24) Huang, G.; Voet, A.; Maglia, G. FraC Nanopores with Adjustable Diameter Identify the Mass of Opposite-Charge Peptides with 44 Da Resolution. *Nat. Commun.* **2019**, *10* (1), 835.
(25) Beesley, J. L.; Woolfson, D. N. The de Novo Design of α-Helical Peptides for Supramolecular Self-Assembly. *Current Opinion in Biotechnology* **2019**, *58*, 175−182.
(26) Shimizu, K.; Mijiddorj, B.; Usami, M.; Mizoguchi, I.; Yoshida, S.; Akayama, S.; Hamada, Y.; Ohyama, A.; Usui, K.; Kawamura, I.; Kawano, R. De Novo Design of a Nanopore for Single-Molecule Detection That Incorporates a β-Hairpin Peptide. *Nat. Nanotechnol* **2022**, *17* (1), 67−75.
(27) Mahendran, K. R.; Niitsu, A.; Kong, L.; Thomson, A. R.; Sessions, R. B.; Woolfson, D. N.; Bayley, H. A Monodisperse Transmembrane α-Helical Peptide Barrel. *Nat. Chem.* **2017**, *9* (5), 411−419.
(28) Krishnan, S.; Satheesan, R.; Puthumadathil, N.; Kumar, K. S.; Jayasree, P.; Mahendran, K. R. Autonomously Assembled Synthetic Transmembrane Peptide Pore. *J. Am. Chem. Soc.* **2019**, *141* (7), 2949−2959.
(29) Krishnan R, S.; Jana, K.; Shaji, A. H.; Nair, K. S.; Das, A. D.; Vikraman, D.; Bajaj, H.; Kleinekathöfer, U.; Mahendran, K. R. Assembly of Transmembrane Pores from Mirror-Image Peptides. *Nat. Commun.* **2022**, *13* (1), 1−13.
(30) R., S. K.; Puthumadathil, N.; Shaji, A. H.; Santhosh Kumar, K.; Mohan, G.; Mahendran, K. R. Designed Alpha-Helical Barrels for Charge-Selective Peptide Translocation. *Chem. Sci.* **2021**, *12* (2), 639−649.
(31) Jia, W.; Hu, C.; Wang, Y.; Gu, Y.; Qian, G.; Du, X.; Wang, L.; Liu, Y.; Cao, J.; Zhang, S.; Yan, S.; Zhang, P.; Ma, J.; Chen, H. Y.; Huang, S. Programmable Nano-Reactors for Stochastic Sensing. *Nat. Commun.* **2021**, *12* (1), 5811.
(32) Bayley, H.; Luchian, T.; Shin, S.-H.; Steffensen, M. B. *Single-Molecule Covalent Chemistry in a Protein Nanoreactor*; Springer, Berlin, 2008; pp 251−277.
(33) Choi, L. S.; Mach, T.; Bayley, H. Rates and Stoichiometries of Metal Ion Probes of Cysteine Residues within Ion Channels. *Biophys. J.* **2013**, *105* (2), 356−364.
(34) Movileanu, L.; Cheley, S.; Howorka, S.; Braha, O.; Bayley, H. Location of a Constriction in the Lumen of a Transmembrane Pore by Targeted Covalent Attachment of Polymer Molecules. *J. Gen. Physiol.* **2001**, *117* (3), 239−251.
(35) Steffensen, M. B.; Rotem, D.; Bayley, H. Single-Molecule Analysis of Chirality in a Multicomponent Reaction Network. *Nat. Chem.* **2014**, *6* (7), 603−607.
(36) Ionescu, S. A.; Lee, S.; Housden, N. G.; Kaminska, R.; Kleanthous, C.; Bayley, H. Orientation of the OmpF Porin in Planar Lipid Bilayers. *ChemBioChem.* **2017**, *18* (6), 554−562.
(37) Braha, O.; Gu, L. Q.; Zhou, L.; Lu, X.; Cheley, S.; Bayley, H. Simultaneous Stochastic Sensing of Divalent Metal Ions. *Nat. Biotechnol.* **2000**, *18* (9), 1005−1007.
(38) Lee, J.; Bayley, H. Semisynthetic Protein Nanoreactor for Single-Molecule Chemistry. *Proc. Natl. Acad. Sci. U. S. A.* **2015**, *112* (45), 13768−13773.
(39) Abdali, N.; Barth, E.; Norouzy, A.; Schulz, R.; Nau, W. M.; Kleinekathöfer, U.; Tauch, A.; Benz, R. Corynebacterium Jeikeium Jk0268 Constitutes for the 40 Amino Acid Long PorACj, Which Forms a Homooligomeric and Anion-Selective Cell Wall Channel. *PLoS One* **2013**, *8* (10), No. e75651.
(40) Movileanu, L.; Cheley, S.; Bayley, H. Partitioning of Individual Flexible Polymers into a Nanoscopic Protein Pore. *Biophys. J.* **2003**, *85* (2), 897−910.
(41) Vikraman, D.; Satheesan, R.; Kumar, K. S.; Mahendran, K. R. Nanopore Passport Control for Substrate-Specific Translocation. *ACS Nano* **2020**, *14* (2), 2285−2295.
(42) De Jesus, A. J.; Allen, T. W. The Role of Tryptophan Side Chains in Membrane Protein Anchoring and Hydrophobic Mismatch. *Biochim Biophys Acta Biomembr* **2013**, *1828* (2), 864−876.
(43) Kong, L.; Harrington, L.; Li, Q.; Cheley, S.; Davis, B. G.; Bayley, H. Single-Molecule Interrogation of a Bacterial Sugar Transporter Allows the Discovery of an Extracellular Inhibitor. *Nat. Chem.* **2013**, *5* (8), 651−659.
(44) Mravic, M.; Thomaston, J. L.; Tucker, M.; Solomon, P. E.; Liu, L.; DeGrado, W. F. Packing of Apolar Side Chains Enables Accurate Design of Highly Stable Membrane Proteins. *Science (1979)* **2019**, *363* (6434), 1418−1423.
(45) Xu, C.; Lu, P.; Gamal El-Din, T. M.; Pei, X. Y.; Johnson, M. C.; Uyeda, A.; Bick, M. J.; Xu, Q.; Jiang, D.; Bai, H.; Reggiano, G.; Hsia, Y.; Brunette, T. J.; Dou, J.; Ma, D.; Lynch, E. M.; Boyken, S. E.; Huang, P. S.; Stewart, L.; DiMaio, F.; Kollman, J. M.; Luisi, B. F.; Matsuura, T.; Catterall, W. A.; Baker, D. Computational Design of Transmembrane Pores. *Nature* **2020**, *585* (7823), 129−134.


https://doi.org/10.1021/jacsau.3c00221
*JACS Au* 2023, 3, 2467−2477

(46) Scott, A. J.; Niitsu, A.; Kratochvil, H. T.; Lang, E. J. M.; Sengel, J. T.; Dawson, W. M.; Mahendran, K. R.; Mravic, M.; Thomson, A. R.; Brady, R. L.; Liu, L.; Mulholland, A. J.; Bayley, H.; DeGrado, W. F.; Wallace, M. I.; Woolfson, D. N. Constructing Ion Channels from Water-Soluble $\alpha$-Helical Barrels. *Nat. Chem.* **2021**, *13* (7), 643−650.
(47) Joh, N. H.; Wang, T.; Bhate, M. P.; Acharya, R.; Wu, Y.; Grabe, M.; Hong, M.; Grigoryan, G.; DeGrado, W. F. De Novo Design of a Transmembrane Zn2+-Transporting Four-Helix Bundle. *Science (1979)* **2014**, *346* (6216), 1520−1524.
(48) Zhang, H.; Li, X.; Hou, J.; Jiang, L.; Wang, H. Angstrom-Scale Ion Channels towards Single-Ion Selectivity. *Chem. Soc. Rev.* **2022**, *51* (6), 2224−2254.
(49) Mantri, S.; Tanuj Sapra, K.; Cheley, S.; Sharp, T. H.; Bayley, H. An Engineered Dimeric Protein Pore That Spans Adjacent Lipid Bilayers. *Nat. Commun.* **2013**, *4* (1), 1725.
(50) Offenbartl-Stiegert, D.; Rottensteiner, A.; Dorey, A.; Howorka, S. A Light-Triggered Synthetic Nanopore for Controlling Molecular Transport Across Biological Membranes. *Angewandte Chemie - International Edition* **2022**, *61* (52), No. e202210886.



https://doi.org/10.1021/jacsau.3c00221
*JACS Au* 2023, 3, 2467−2477